Electrochemical and Solid-State Letters, **15** (4) K35-K39 (2012)
1099-0062/2012/15(4)/K35/5/$28.00 © The Electrochemical Society

Anomalous Oxidation Resistance of "Core-Only" Copper Nanoparticles Electrochemically Grown on Gold Nanoislands Prefunctionalized by 1,4-phenylene Diisocyanide

Youngku Sohn,[a] Debabrata Pradhan,[b] Liyan Zhao, and K. T. Leung[z]

WATLab, and Department of Chemistry, University of Waterloo, Waterloo, Ontario N2L 3G1, Canada

Copper was electrodeposited on bare and pre-functionalized Au nanoislands with 1,4-phenylene diisocyanide (PDI, $^{-}C{\equiv}N^{+}{-}C_6H_4{-}N^{+}{\equiv}C^{-}$), on a Si(100) substrate. The electrodeposited Cu nanoparticles on bare Au nanoislands are found to consist of a Cu core and a Cu_2O shell with a CuO overlayer. For Cu nanoparticles electrodeposited on Au nanoislands pre-functionalized with PDI, the metallic Cu core is covered by a barely detectable Cu_2O overlayer, without any evidence of the CuO shell. PDI-functionalization of the Au nanoislands could be used to suppress the Cu oxidation and significantly alter the interfacial electronic nature of Cu on PDI-functionalized Au nanoislands.
 [DOI: 10.1149/2.006205esl]

Manuscript submitted November 15, 2011; revised manuscript received January 17, 2012. Published February 9, 2012.

Hybrid (bimetallic or alloy) nanoparticles have attracted a lot of attention because of their potential applications in many industrial processes, including efficient catalysts and cell electrodes.[1–7] Their chemical and physical properties greatly depend on the relative composition of the constituent metals, their size and surface structure.[8–10] Much effort has been devoted to producing different types of bimetals by varying different preparation methods.[11–16] By adding an appropriate metal to another metal, it is often possible to achieve an enhancement in the catalytic, electrical and other property of the bimetallic material.[17–20] Gold is one of the most popular metals that has played an important role in improving the properties of bimetallic nanoparticles. For example, it was found that the deactivation process (known as catalyst poisoning) of Ni catalysts for a steam-reforming reaction can be minimized by adding a small amount of Au onto Ni.[4,21] In the acetoxylation reaction of ethylene to produce vinyl acetate, Chen et al. found that the catalytic activity of Pd could be greatly enhanced upon addition of a small amount of Au.[19] The change in chemical properties of Pd such as catalytic activity has been attributed to geometric and/or electronic effects produced by the second metal.[9,10,19] The addition of another metal can therefore be used to introduce new desirable properties in catalysts or electronic electrodes.

In the present work, we electrodeposit Cu nanoparticles on Au nanoislands (NIs) and study the changes in the electronic properties of Cu nanoparticles on bare and functionalized Au NIs. Although the noble metals Cu and Au both exhibit the same $(n\text{-}1)d^{10}ns^1$ electron configuration, Cu nanoparticles are easily oxidized while the Au support is fairly inert. Here, we demonstrate that Cu nanostructures could be made highly resistant to oxidation by modifying the Au NI substrate with 1,4-phenylene diisocyanide functionalization. It has been reported that the isocyanide ($-N^{+}{\equiv}C^{-}$) group in an aromatic isocyanide ($Ar{-}N^{+}{\equiv}C^{-}$) strongly binds to both Au and Cu surfaces. In particular, Sohn and White found that σ–bonded linear Ar–N≡C–Au and σ/π–bonded bent Ar–N=C=Cu forms are dominant for Au(111) and Cu(111) surfaces, respectively.[22] The present work demonstrates, for the first time, that appropriate functionalization of the metallic substrate by an isocyanide group could significantly affect the properties of the second metal in a bimetallic nanosystem.

Experimental

The electrochemical deposition of Cu on a Au NI template was performed in a conventional three-electrode cell using a CH Instruments 660A electrochemical workstation. A standard Ag/AgCl electrode and a platinum wire were used as the reference and counter electrodes, respectively. A single-side-polished, rectangular (15×2.5 mm^2), p-type Si(100) chip (0.4-mm-thick, with a resistivity of 1.0–1.5 mΩ · cm) was used as the support for preparing the Au NI template by sputter-deposition of Au using a magnetron sputter-coater (Denton Desk II) followed by thermal annealing. Details about controlling the size of the Au NIs by varying the sputter-deposition time and the post-annealing temperature have been given in our recent work.[23] The resulting Au NI template, with size-controllable Au NIs, was then used as the working electrode for the Cu electrodeposition. In addition to the pristine Au NIs, the Au NIs were also functionalized by dipping in a 1.0 mM 1,4-phenylene diisocyanide (PDI, $^{-}C{\equiv}N^{+}{-}C_6H_4{-}N^{+}{\equiv}C^{-}$, 99% purity, Sigma-Aldrich) toluene solution for 12 h, followed by thorough rinsing with fresh toluene. Before PDI functionalization or direct Cu deposition, the bare Au NI template was dipped in a 1% HF solution for 30 s to reduce the thick Si oxide layer arising from the post-annealing step in synthesizing the template.[23] Cu was deposited on both the pristine Au NIs and the PDI-functionalized Au NIs potentiostatically by amperometry in a deoxygenated 10.0 mM $Cu(SO_4)_2 \cdot 6H_2O$ aqueous electrolyte solution mixed with 100 mM $NaClO_4$ used as a supporting electrolyte. After the electrodeposition at an applied potential of −0.6 V (vs. Ag/AgCl) for 10 s, we thoroughly rinsed the sample with Millipore water, and dried under nitrogen stream before further analysis. No S, Cl, and Na from the residual electrolytes were detectable by X-ray photoelectron spectroscopy.

The surface morphology and elemental composition were characterized by scanning electron microscopy (SEM) and energy-dispersive X-ray analysis, respectively, in a LEO field-emission scanning electron microscope. The chemical-state composition of the sample was analyzed by X-ray photoelectron spectroscopy (XPS) as a function of Ar ion sputtering time. The XPS depth-profiling experiments were performed by using a Thermo-VG Scientific ESCALab 250 microprobe with a monochromatic Al Kα X-ray source (1486.6 eV) and a typical energy resolution of 0.4–0.5 eV full width at half maximum (fwhm). The Ar ion sputtering was conducted over a rastered sample area of 3×3 mm^2 at 3.0 keV ion beam energy and a sample current density of 0.3–0.4 μA mm^{-2}.

Results and Discussion

Figure 1 shows the SEM images of bare Au NIs on Si(100) (with a size distribution of 20–100 nm),[23] and the Cu nanoparticles electrodeposited on Au NIs without and with PDI functionalization at −0.6 V (vs. Ag/AgCl) for 10 s. Because a very thick Si oxide layer often formed during the post-annealing step in the preparation of the Au NIs, Cu could not be efficiently electrodeposited on the Au NIs. To

[a] Present address: Department of Chemistry, Yeungnam University, Gyeongsan, Gyeongbuk 712-749, South Korea.
[b] Present address: Materials Science Center, Indian Institute of Technology, Kharagpur, West Bengal 721 302, India.
[z] Email: tong@uwaterloo.ca

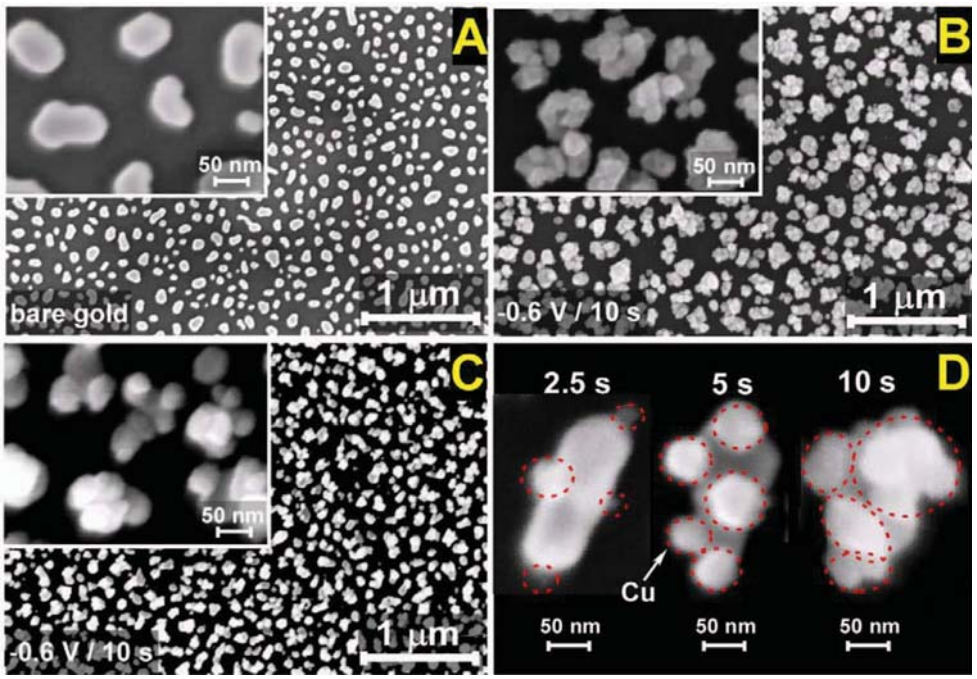

Figure 1. SEM images (with magnified views in insets) of (A) bare Au nanoislands, and Cu nanoparticles electrodeposited at −0.6 V (vs. Ag/AgCl) for 10 s on (B) bare and (C) 1,4-phenylene diisocyanide-functionalized Au nanoislands. (D) Magnified SEM images of growth evolution of Cu nanoparticles on a functionalized Au nanoisland with increasing deposition time.

overcome this, we reduced the thickness of the oxide layer by dipping in a 1% HF solution for 30 s. By controlling the thickness of the oxide layer, we were able to deposit Cu mainly onto the Au NIs and scarcely on the less conducting oxidized Si surface. On the bare Au NIs (Figure 1A), distorted cuboid Cu nanoparticles are found to completely cover the entire Au NIs, creating the appearance of a distorted nanoparticle cluster (Figure 1B). Upon PDI-functionalization of the Au NIs, the amount of deposited Cu nanoparticles is found to be reduced noticeably (not shown) and not all the Au NIs are completely covered by the Cu nanoparticles (Figure 1C). Furthermore, increasing the deposition time caused the Cu nanoparticles (seen as the brighter spots marked in broken circles in Figure 1D) on the PDI-functionalized Au NIs to grow bigger, along with an increase in the number density. Without the Au NIs, Cu could also be electrodeposited efficiently on a H–terminated or native-oxide covered Si substrate.[24] As described in our recent work,[25] the shapes and sizes of the electrodeposited Cu nanoparticles could be controlled by precisely changing the electrolyte concentration and deposition time (for a given deposition potential).

Figure 2 shows the corresponding depth-profiling XPS spectra of the Cu $2p_{3/2}$, Cu LMM Auger, O 1s, and Au 4f regions of Cu nanoparticles electrodeposited on bare and PDI-functionalized Au NIs (shown in Figures 1B and 1C, respectively). For the as-deposited Cu nanoparticles on bare Au NIs (before Ar ion sputtering, Figure 2 upper), the dominant Cu $2p_{3/2}$ peak at 932.8 (±0.1) eV can be assigned to Cu_2O (cuprous oxide) and/or metallic Cu,[25] while the considerably weaker feature at 934.7 eV, with its corresponding shake-up peak at ∼942.0 eV (not shown), is attributed to CuO (cupric oxide).[26–29] The binding energy (BE) of the Cu $2p_{3/2}$ feature for CuO is ∼2 eV higher than those for Cu_2O and Cu, with the BE difference between the latter two found to be negligibly small.[26] To discriminate Cu_2O from Cu, we examine the corresponding Cu LMM Auger and O 1s BE spectra.[26,27] The broad Cu LMM Auger peak observed at 916.8 eV kinetic energy (or 569.8 eV BE with Al K_α) can only be assigned to Cu_2O but not to Cu, given that the corresponding Cu LMM feature for Cu is 1.4 eV higher.[26,27] Although the Cu LMM Auger peak for CuO is also found to be between 916.0 and 917.0 eV, its contribution to the Cu LMM band is expected to be rather small given the observed weak intensity of the corresponding Cu $2p_{3/2}$ photopeak at 934.7 eV.[25] In addition, the prominent O 1s peak at 532.4 eV BE can be assigned predominantly to silicon oxide (with only a rather weak contribution from CuO), while the well-defined, weaker O 1s feature at 530.6 eV can be unambiguously attributed to Cu_2O.[25]

Upon just 5 s of Ar ion sputtering, the weak Cu $2p_{3/2}$ peak at 934.7 eV BE for CuO was completely removed, while the intense Cu $2p_{3/2}$ peak at 932.8 eV with a fwhm of 1.3_3 eV has become more intense, likely due to the removal of the carbonaceous layer arising from sample handling in ambient conditions. Given that we observe (in a separate experiment) the Cu $2p_{3/2}$ peak for a clean Cu(100) single crystal at 932.9 eV, with a fwhm of 1.0 eV, while that for Cu_2O has been reported at 932.6 eV,[25] we perform further analysis in order to determine the nature of these Cu nanoparticles. The corresponding O 1s peak at 532.4 eV for silicon suboxide and that at 530.6 eV for Cu_2O are well resolved. To calculate the surface composition of Cu to O, we integrate the O 1s feature at 530.6 eV and the Cu 2p feature and divide the resulting XPS areas by their corresponding relative sensitivity factors (0.66 for O 1s and 6.3 for Cu 2p).[30] We obtain a Cu:O ratio of 2.2, which indicates that the Cu $2p_{3/2}$ peak after the 5 s of sputtering is mainly due to Cu_2O, with only a minor contribution to the Cu signal from the metallic Cu core. The calculated surface composition also confirms our assignment of the broad Auger LMM feature at 916.8 eV kinetic energy primarily to Cu_2O (and not CuO). Upon 15 s of sputtering, the two O 1s peaks are found to further decrease in intensity as expected, and the corresponding surface composition is estimated to be $Cu_{2.6}O_1$. This indicates that the Cu_2O shell has become thinner, which in turn increases the relative Cu $2p_{3/2}$ sampling contribution from the metallic Cu core (thereby increasing the observed relative Cu contribution correspondingly). For the Cu LMM Auger line, the emergence of a peak at 918.2 eV kinetic energy associated with metallic Cu is clearly observed. With increasing sputtering time, the Cu LMM Auger feature for Cu_2O at 916.8 eV decreases in intensity, while that of metallic Cu at 918.2 eV becomes more intense. After 120 s of sputtering, the O 1s peak for Cu_2O at 530.6 eV is completely removed, leaving behind a prominent Cu LMM peak at 918.2 eV kinetic energy attributable to the metallic Cu core. It has been suggested that reduction of CuO to Cu_2O could

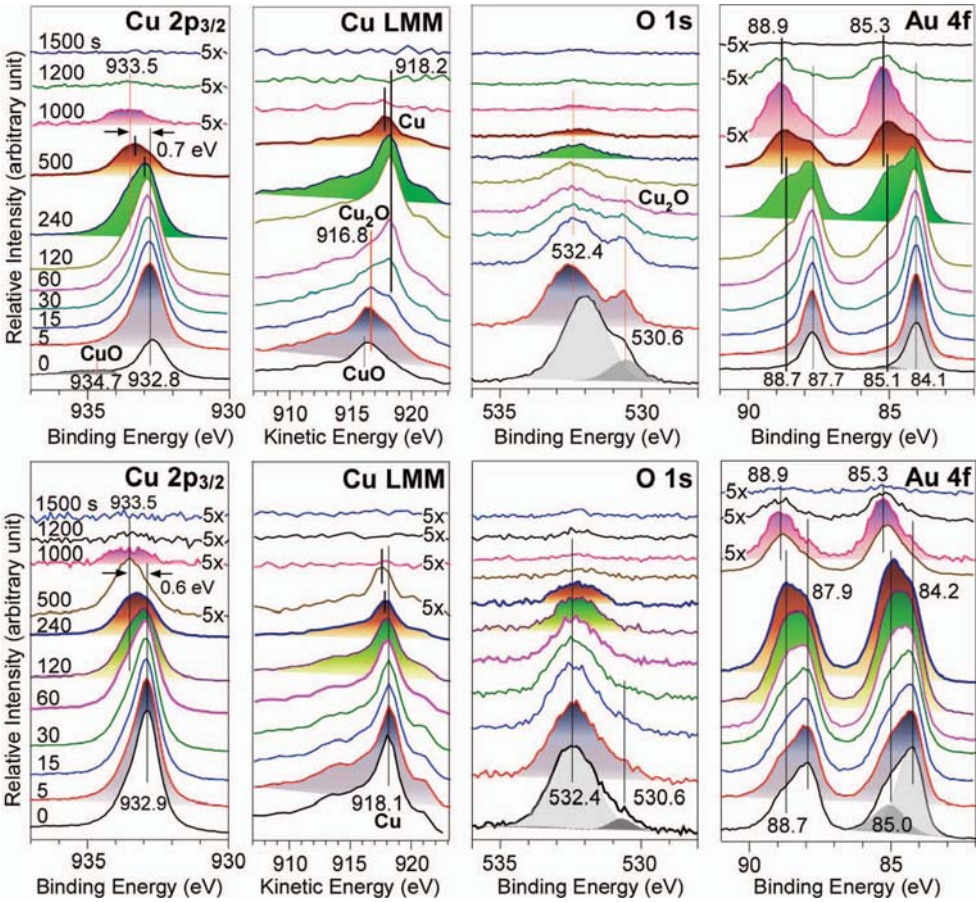

Figure 2. XPS spectra of Cu $2p_{3/2}$, Cu LMM Auger, O 1s, and Au 4f regions for Cu nanoparticles as-electrodeposited on supported bare (upper panel) and 1,4-phenylene diisocyanide-functionalized (lower panel) Au nanoislands, and upon sputtering for 5, 15, 30, 60 120, 240, 500, 1000, 1200, and 1500 s.

be induced by Ar ion sputtering with 3–5 keV ion beam energy.[31] However, since the Cu $2p_{3/2}$ peak of CuO at 934.7 eV is very weak while the Cu_2O/Cu peak at 932.8 eV is dominant for the as-deposited sample, we could rule out the sputtering-induced reduction of CuO to Cu_2O in our discussion.

Interestingly, sputtering for 120 s also causes the Cu $2p_{3/2}$ peak to become broader and asymmetric to higher BE. Further sputtering to 500 s and to 1000 s considerably reduces the Cu $2p_{3/2}$ feature with further broadening in width, revealing a new Cu $2p_{3/2}$ peak (with 1.6 eV fwhm) at 933.5 eV, i.e. ~0.7 eV higher in BE than that of metallic Cu (932.8 eV). This shifted Cu $2p_{3/2}$ feature could be due to the emergence of a new species, possibly Cu silicide or Au-Cu alloy or both, and/or to a quantum size effect (as the Cu nanoparticles are becoming smaller with increasing sputtering time). In our recent work on Cu nanoparticles deposited directly on Si(100),[25] our depth-profiling XPS study showed that the metallic Cu core is also covered by Cu_2O. We also found a BE shift in the Cu $2p_{3/2}$ peak by +0.3 eV, with the peak width (1.1 eV fwhm) becoming smaller, but these changes occurred in the transition region from the Cu_2O shell to metallic Cu core.[25,26] Paszti et al. also performed similar experiments on a thin Cu film grown on Si(100),[32] and they found that the Cu $2p_{3/2}$ peak broadens and shifts by +0.4 eV with increasing sputtering time, without any indication of Cu oxide formation. They attributed the XPS result not to the formation of Cu silicide but to a quantum size effect. As for the possibility of Au-Cu alloy formation, it was reported that no intermixing occurs at the Cu-Au interface for Cu islands electrodeposited on Au(111), while for the thermally evaporated Cu on Au under ultrahigh vacuum condition, there was evidence of intermixing.[33] For Cu-Au alloys prepared under various different conditions,[34–40] it has commonly been found that the Cu $2p_{3/2}$ BE decreases while the Au $4f_{7/2}$ BE increases, relative to those of the metallic Cu and Au, respectively. In particular, Santra et al. observed that the BE of the Cu $2p_{3/2}$ peak shifts by −0.25 eV for thermally evaporated Cu on a Au substrate.[38] Kim et al. reported a Cu $2p_{3/2}$ peak at 933.4 eV and a Au $4f_{7/2}$ peak at 85.0 eV for $AuCu_3$ alloy nanoparticles (with an average size of 3 nm) prepared from a mixed $Cu(NO_3)_2$ and $HAuCl_4$ solution,[40] which correspond to a −0.2 eV and a +1.0 eV BE shifts from the respective Cu 2p and Au 4f peaks found for the Cu and Au nanoparticles, respectively. According to a theoretical calculation by Lekka et al., the Cu atoms gain 0.03 e^- per atom while the Au atoms lose 0.13 e^- per atom, with respect to their respective pure metallic forms, upon formation of the $AuCu_3$ alloy.[41] The +0.7 eV BE shift found for the new Cu $2p_{3/2}$ feature at 933.5 eV would therefore reject the notion of formation of Cu silicide or Au-Cu alloy, which leaves the formation of a new chemical species or initial-state quantum size effect or both as the only plausible assignment(s).

In order to further resolve these two possibilities, we examine the depth-profiling Au 4f spectra (Figure 2, upper), which evidently change in a very similar fashion as that found for Au NIs on a Si(100) substrate shown in our recent work.[23] Before sputtering, a dominant metallic Au $4f_{7/2}$ peak at 84.1 eV and a minor peak (Au silicide) at 85.1 eV are observed. As the sputtering time increases, the Au $4f_{7/2}$ peak at 85.1 eV corresponding to Au silicide becomes prominent.[23] The estimated Cu/Au stoichiometric ratios upon sputtering for 500 s, 1000 s, and 1200 s are 1/1.1, 1/2.9 and 1/3.6, respectively. The Cu/Au ratio decreases with increasing sputtering time due to the efficient removal of the top-lying Cu species than the underlying Au NIs. Upon 1200 s of sputtering, all the Cu 2p features have evidently been removed and only a weak Au $4f_{7/2}$ peak of Au silicide remains. The new Cu $2p_{3/2}$ feature with a +0.7 eV BE shift observed above could

be due to initial-state electronic perturbation by Au and/or Si in the quantum size region.

Figure 2 (lower) shows the depth-profiling XPS spectra of Cu $2p_{3/2}$, Cu LMM Auger, O 1s, and Au 4f of Cu nanoparticles electrodeposited on PDI-functionalized Au NIs (shown in Figure 1C). The as-deposited sample exhibits a single Cu $2p_{3/2}$ peak at 932.9 eV, with a fwhm of 1.2_8 eV, the peak position and width of which remain unchanged upon sputtering for up to 30 s. Further sputtering to 60 s and 120 s reduces the intensity of the Cu $2p_{3/2}$ peak and broadens the width to 1.4_2 eV and 1.4_8 eV fwhm, respectively, while the peak profile becomes more asymmetric. The asymmetric peak appears to contain at least two different species as discussed previously. Upon sputtering for 240 s, the photopeak position notably shifts to 933.2 eV, and the width further broadens to 1.5_2 eV fwhm. Similarly, the Cu LMM Auger feature also appears to shift to a lower kinetic energy position. After 500 s of sputtering, the Cu $2p_{3/2}$ photopeak becomes symmetric and appears at 933.5 eV, with a width of 1.5 eV fwhm. Except for the rather stable intensity found for the Cu nanoparticles on PDI-functionalized Au NIs in the initial sputtering region (< 30 s), the subsequent spectral evolution with sputtering time (Figure 2, lower) therefore follows that found for Cu on bare Au NIs (Figure 2, upper).

To properly assign the Cu $2p_{3/2}$ peak at 932.9 eV (i.e. to metallic Cu or Cu_2O or both), we again examine the corresponding Cu LMM Auger spectrum, which exhibits a prominent metallic Cu feature at 918.1 eV kinetic energy, with no sign of Cu_2O or CuO (at 916.8 eV).[26,27] The peak position of this metallic Cu Auger feature also shows no discernible change with increasing sputtering time. Given that the Cu_2O shell could be too thin to be identified from its Cu $2p_{3/2}$ and Cu LMM Auger signals due to the overwhelming contribution from the metallic Cu core, we carefully examine the O 1s spectrum in order to identify the existence of Cu_2O. Assuming that Cu_2O is present, we fit the broad O 1s XPS spectrum of the as-deposited sample with two peaks at 532.4 eV and 530.6 eV, corresponding to silicon oxide and Cu_2O respectively (Figure 2, lower), and estimate the Cu:O ratio to be 23:1. This confirms that the amount of Cu_2O on the Cu nanoparticles is negligibly small on the PDI-functionalized Au NIs, essentially within the detection limit, and that the Cu nanoparticles so produced may be regarded as "shell-less", core-only metallic nanoparticles that are extremely resistant to oxidation. This is in marked contrast to the considerable amount found on the as-deposited Cu nanoparticles on bare Au NIs (with a Cu:O ratio of 2.2:1), which requires 120 s of sputtering for complete removal (Figure 2, upper). Not surprisingly, the spectral evolution of the predominant silicon oxide O 1s feature (at 532.4 eV) for the Cu nanoparticles on PDI-functionalzed Au NIs follows that on bare Au NIs with increasing sputtering time.

The Au 4f XPS spectra of Cu nanoparticles on PDI-functionalized Au NIs (Figure 2, lower) is remarkably different from that on bare Au NIs (Figure 2, upper). In particular, the Au $4f_{7/2}$ band for the as-deposited Cu nanoparticles on PDI-functionalized Au NIs appears asymmetric and can be fitted with two peaks at 84.2 eV and 85.0 eV, corresponding to metallic Au and Au silicides, respectively, of the regions of the functionalized Au NIs not covered by the Cu nanoparticles. The AuSi component becomes comparable in intensity to the metallic Au component as the sputtering time increases from 60 s to 120 s and 240 s. Sputtering for over 500 s appears to remove most of the metallic Au component, and the corresponding spectral evolution with sputtering time (Figure 2, lower) follows that on bare Au NIs (Figure 2, upper). The Au $4f_{7/2}$ BE difference between Au and AuSi for the PDI-functionalized Au NIs is 0.8 eV (Figure 2, lower), which is 0.2 eV smaller than that (1.0 eV) found on Au NIs without PDI functionalization (Figure 2, upper). In addition, for the as-deposited PDI-functionalized sample the Au 4f intensity of the AuSi component (at 85.0 eV) is substantial, when compared to that for bare Au NIs. The greater intensity of AuSi for PDI-functionalized Au NI sample could be due to that some of the exposed AuSi (during the HF treatment – see Experimental Section) upon functionalized by PDI become less favorable for Cu nanoparticle growth, compared to those exposed AuSi regions not functionalized by PDI. Furthermore, the Au $4f_{7/2}$ photopeak of the AuSi component appears to further shift to a higher BE at 85.3 eV (Figure 2) upon sputtering for more than 500 s. This minor BE shift could be due to a quantum size effect.

Evidently, the adsorbed PDI molecules on Au NIs appear to act as a Cu oxidation suppressor (or a retardant), protecting the Cu surface, during the subsequent Cu deposition. Some discussion on the mechanism of the observed oxidization-resistant property of Cu nanoparticles on PDI-functionalized Au NIs is in order. Here, we propose two hypothetical growth modes: a Cu-on-Au direct growth (or Cu penetration) model,[42,43] and a Cu-on-isocyanide indirect growth model.[43,44] We examined the cyclic voltammetry and deposition current vs time data of Cu on bare Au and on PDI-functionalized Au NIs. For Cu electrodeposition on bare Au, it appears that the current vs time curve shows an instantaneous island growth mode at a less negative potential (e.g, −0.4 eV vs Ag/AgCl). On the other hand, the current vs time curve for Cu on PDI-functionalized Au exhibits a two-stage growth mode at a less negative potential: an apparently instantaneous homogeneous Au growth on top of (or underneath) PDI followed by Cu island growth. At a more negative potential (e.g, −1.2 eV vs Ag/AgCl), the two growth modes of Cu on bare and on PDI-functionalized Au NIs appear to be very similar. In the first scenario, a Cu ion could penetrate through the PDI adlayer on the Au NI and deposits directly on the Au NI surface not covered by PDI (pinholes) during the initial stage of electrodeposition. The neighboring PDI molecules could cover the deposited Cu atom, in effect shielding it from oxidation. As more Cu atoms penetrate through the PDI layer to continue the nucleation process, the Cu nanodeposit grows bigger and starts to cover the PDI molecules (Cu-on-Au "mushroom" direct growth). In the second scenario, the Cu ion could interact directly with the pendant isocyanide groups of the PDI adlayer (through formation of a strong Cu-isocyanide chemical bond),[22,45] which also leads to Cu nanodeposits covering the PDI adlayer (Cu-on-isocynaide indirect growth). Both of these scenarios could account for the lack of discernible N 1s signal found for the as-deposited sample in our XPS experiments. Furthermore, because PDI is an aromatic isocyanide molecule with $–N^+{\equiv}C^-$ functional groups, in which electrons are fully delocalized over the backbone, the positively charged Cu^{2+} ions are more attracted to the more negatively charged PDI-modified Au NI surface than the bare Au NI surface, leading to preferential growth on the PDI-modified Au NIs. This more negatively charged PDI-functionalized Au surface also leads to a more gradual potential change of the Helmholtz and diffusion layers with distance from the surface than that for Cu nanoparticle deposition on the bare Au NIs.[46] The more negatively charged surface of the Cu nanodeposits on PDI-modified Au NIs could retard oxygen diffusion, thereby suppressing Cu oxidation. As the Cu nanodeposits grow in size, the effect of the negatively charged interface becomes less and Cu oxidation will consequently approach that on bare Au NI. To further evaluate these models, we are conducting further studies on metal electrodeposition on various metal nanoisland templates pre-functionalized by 1,4-phenylene diisocyanide.

Summary

The interfacial electronic structures of electrodeposited Cu nanoparticles on bare Au NIs are dramatically different from that on PDI-functionalized Au NIs, as elucidated by our SEM and XPS analyses. On the basis of our depth-profiling XPS data (for Cu 2p, Cu LMM Auger, and O 1s), a Cu nanoparticle on bare Au NIs could be described as a Cu-Cu_2O-CuO core-shell-skin nanostructure, while that on PDI-functionalized Au NIs is mainly a metallic Cu core covered by an ultrathin layer of Cu_2O, with no detectable CuO (Figure 3). The remarkable lack of discernible oxidation of Cu on the PDI-functionalized Au can be explained by a Cu-on-Au direct growth model, or a Cu-on-isocyanide indirect growth model that suppresses oxygen diffusion thereby retarding Cu oxidation. The PDI molecule therefore acts as not only an electronic coupling linker between the Cu nanodeposit and the Au NI, but also a highly effective oxidation inhibitor for the deposited Cu nanostructure. For both Cu

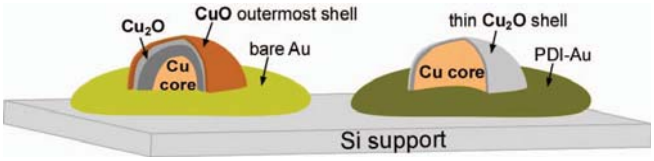

Figure 3. Chemical nature of Cu nanoparticles electrochemically grown on bare Au and PDI-functionalized Au nanoislands.

nanoparticles on bare and PDI-functionalized Au NIs, we also observed that the Cu $2p_{3/2}$ peak broadens and shifts to a higher BE by 0.7 ($\pm$ 0.1) eV than that of metallic Cu, upon sufficient sputtering for size reduction. Given that we found no evidence for the formation of Cu silicide and Au-Cu alloy, the observed BE shift could be attributed to an initial-state quantum size effect. Our present result therefore shows that appropriate organic functionalization of the metallic Au NI could have a significant effect on the chemical properties of Cu nanostructures in this bimetallic nanosystem. This fundamental finding could be potentially used in a molecular-electronics application involving an appropriate molecule sandwiched by two different metal electrodes without risk of electrode surface oxidation. In addition, the present work also offers new insights into the interfacial electronic structures, the chemical bonding, and the interactions between the metal contacts and the sandwiched molecule.

Acknowledgment

This research was supported by the Natural Sciences and Engineering Research Council of Canada.

References

1. N. Toshima and T. Yonezawa, *New J. Chem.*, **22**, 1179 (1998).
2. C. T. Campbell, *Annu. Rev. Phys. Chem.*, **41**, 775 (1990).
3. M. T. M. Koper, *Surf. Sci.*, **548**, 1 (2004).
4. A. T. Bell, *Science*, **299**, 1688 (2003).
5. L. Guczi, *Catal. Today*, **101**, 53 (2005).
6. B. F. G. Johnson, *Coord. Chem. Rev.*, **190-192**, 1269 (1999).
7. D. Astruc, F. Lu, and J. R. Aranzaes, *Angew. Chem., Int. Ed.*, **44**, 7852 (2005).
8. M.-C. Daniel and D. Astruc, *Chem. Rev.*, **104**, 293 (2004).
9. C. N. R. Rao, G. U. Kulkarni, P. J. Thomas, and P. P. Edwards, *Chem. Soc. Rev.*, **29**, 27 (2000).
10. M. Haruta, *Catal. Today*, **36**, 153 (1997).
11. D.-H. Chen and C.-J. Chen, *J. Mater. Chem.*, **12**, 1557 (2002).
12. S. Devarajan, P. Bera, and S. Sampath, *J. Colloid Interface Sci.*, **290**, 117 (2005).
13. B. L. Cushing, V. L. Kolesnichenko, and C. J. O'Connor, *Chem. Rev.*, **104**, 3893 (2004).
14. A. K. Sra and R. E. Schaak, *J. Am. Chem. Soc.*, **126**, 6667 (2004).
15. C. J. Murphy, T. K. Sau, A. M. Gole, C. J. Orendorff, J. Gao, L. Gou, S. E. Hunyadi, and T. Li, *J. Phys. Chem. B*, **109**, 13857 (2005).
16. J. D. Aiken III and R. G. Finke, *J. Mol. Catal. A*, **145**, 1 (1999).
17. J. H. Liu, A. Q. Wang, H. P. Lin, and C. Y. Mou, *J. Phys. Chem. B*, **109**, 40 (2005).
18. L. Prati, A. Villa, F. Porta, D. Wang, and D. Su, *Catal. Today*, **122**, 386 (2007).
19. M. Chen, D. Kumar, C.-W. Yi, and D. W. Goodman *Science*, **310**, 291 (2005).
20. L. Guczi *Catal. Today* **101**, 53 (2005).
21. F. Besenbacher, I. Chorkendorff, B. S. Clausen, B. Hammer, A. M. Molenbroek, J. K. Nørskov, and I. Stensgaard, *Science*, **279**, 1913 (1998).
22. Y. Sohn and J. M. White, *J. Phys. Chem. C*, **111**, 5006 (2008).
23. Y. Sohn, D. Pradhan, A. Radi, and K. T. Leung, *Langmuir*, **25**, 9557 (2009).
24. X. J. Zhou, A. J. Harmer, N. F. Heinig, and K. T. Leung *Langmuir*, **20**, 5109 (2004).
25. A. Radi, D. Pradhan, Y. Sohn, and K. T. Leung, *ACS Nano*, **4**, 1553 (2010).
26. *Handbook of X-ray Photoelectron Spectroscopy*, J. Chastain, Ed. (Perkin-Elmer Corporation, Eden Prairie, Minnesota, 1992).
27. M. M. Sung, K. Sung, C. G. Kim, S. Sun, S. S. Lee, and Y. Kim, *J. Phys. Chem. B*, **104**, 2273 (2000).
28. T. H. Fleisch and G. J. Mains, *Appl. Surf. Sci.*, **10**, 51 (1982).
29. J. Ghijsen, L. H. Tjeng, J. van Elp, H. Eskes, J. Westerink, G. A. Sawatzky, and M. T. Czyzyk, *Phys. Rev. B*, **38**, 11322 (1988).
30. *Practical Surface Analysis. Vol. 1. Auger and X-ray Photoelectron Spectroscopy D*, D. Briggs and M. P. Seah (Ed.), (John Wiley & Sons, U. K. Chichester, 1990).
31. G. Panzner, B. Egert, and H. P. Schmidt, *Surf. Sci.*, **151**, 400 (1985).
32. Z. Pászti, G. Petö, Z. E. Horváth, A. Karacs, and L. Guczi, *J. Phys. Chem. B*, **101**, 2109 (1997).
33. X. Zhao, P. Liu, J. Hrbek, J. A. Rodriguez, and M. Perez, *Surf. Sci.*, **592**, 25 (2005).
34. C. Sangregorio, M. Galeotti, U. Bardi, and P. Baglioni, *Langmuir*, **12**, 5800 (1996).
35. W. Eberhardt, S. C. Wu, R. Garrett, D. Sonericker, and F. Jona, *Phys. Rev. B*, **31**, 8285 (1985).
36. M. Kuhn and T. K. Sham, *Phys. Rev. B*, **49**, 1647 (1994).
37. T. K. Sham, Y. M. Yiu, M. Kuhn, and K. H. Tan, *Phys. Rev. B*, **41**, 11881 (1990).
38. A. K. Santra and C. N. R. Rao, *Appl. Surf. Sci.*, **84**, 347 (1995).
39. T.-H. Kao, J.-M. Song, I.-G. Chen, T.-Y. Dong, and W.-S. Hwang, *Nanotech.*, **18**, 435708 (2007).
40. M.-J. Kim, H.-J. Na, K. C. Lee, E. A. Yoo, and M. Lee, *J. Mater. Chem.*, **13**, 1789 (2003).
41. Ch. E. Lekka, N. Bernstein, M. J. Mehl, and D. A. Papaconstantopoulos, *Appl. Surf. Sci.*, **219**, 158 (2003).
42. P. Lu and A. V. Walker, *Langmuir*, **23**, 12577 (2007).
43. H. Hagenström, M. A. Schneeweiss, and D. M. Kolb, *Langmuir*, **15**, 7802 (1999).
44. O. Seitz, M. Dai, F. S. Aguirre-Tostado, R. M. Wallace, and Y. J. Chabal, *J. Am. Chem. Soc.*, **131**, 18159 (2009).
45. Y. Sohn and J. M. White, *J. Phys. Chem. C*, **111**, 7816 (2007).
46. R. Memming, *Semiconductor Electrochemistry*, (W. Wiley-VCHeinheim, Germany, 2002).